

Crossover from regular to irregular behavior in current flow through open billiardsKarl-Fredrik Berggren,¹ Almas F. Sadreev,^{1,2} and Anton A. Starikov^{1,2}¹*Department of Physics and Measurement Technology, Linköping University, S-581 83 Linköping, Sweden*²*Kirensky Institute of Physics, 660036, Krasnoyarsk, Russia*

(Received 22 December 2001; published 26 July 2002)

We discuss signatures of quantum chaos in terms of distributions of nodal points, saddle points, and streamlines for coherent electron transport through two-dimensional billiards, which are either nominally integrable or chaotic. As typical examples of the two cases we select rectangular and Sinai billiards. We have numerically evaluated distribution functions for nearest distances between nodal points and found that there is a generic form for open chaotic billiards through which a net current is passed. We have also evaluated the distribution functions for nodal points with specific vorticity (winding number) as well as for saddle points. The distributions may be used as signatures of quantum chaos in open systems. All distributions are well reproduced using random complex linear combinations of nearly monochromatic states in nominally closed billiards. In the case of rectangular billiards with simple sharp-cornered leads the distributions have characteristic features related to order among the nodal points. A flaring or rounding of the contact regions may, however, induce a crossover to nodal point distributions and current flow typical for quantum chaos. For an irregular arrangement of nodal points, as for example in the Sinai billiard, the quantum flow lines become very complex and volatile, recalling chaos among classical trajectories. Similarities with percolation are pointed out.

DOI: 10.1103/PhysRevE.66.016218

PACS number(s): 05.45.Mt, 05.60.Gg, 73.23.Ad

I. INTRODUCTION

Billiards play a predominant role in the study of classical and quantum chaos (see, e.g., Ref. [1]). Indeed, the nature of quantum chaos in a specific system is traditionally inferred from its classical counterpart. Hence one may ask if quantum chaos is to be understood solely as a phenomenon that relates to the classical limit, or if there are some intrinsic quantal phenomena, which may contribute to irregular behavior in the quantum domain. This is one of the questions we raise in connection with quantum transport through regular and irregular electron billiards. We will assume that we deal with billiards that are ballistic. In practice this situation is well met when the mean free path is very long and exceeds the dimensions of, for example, electron billiards fabricated in high-mobility GaAs/AlGaAs [2].

The seminal studies by McDonnell and Kaufman [3] of the morphology of eigenstates in a closed Bunimovich stadium have revealed characteristic complex patterns of disordered, unidirectional, and noncrossing nodal lines [4,5]. Such features have also been observed experimentally for microwave cavities [1,6] and acoustic resonators [7].

Here we will discuss what will happen to patterns like these when ideal leads are attached to a billiard, regular or irregular, and an electric current is induced through the the cavity by a small applied voltage between source and drain. The wave function ψ is then a scattering state with both real and imaginary parts,

$$\psi(x,y) = u(x,y) + iv(x,y), \quad (1)$$

which gives rise to two separate sets of noncrossing nodal lines at which either u or v vanish. How will the patterns of nodal lines evolve as the energy is increased, i.e., more scattering channels are opened? Could they tell us something

about how attached leads perturb the wave function and how, for example, an initially regular billiard might eventually turn into a chaotic one as the number of open modes increase and/or the shapes of contact regions are modified? The nodal points (NPs) at which the scattering wave function equals zero, i.e., the points at which the two sets of nodal lines intersect because $u = v = 0$, carry important information in this respect. While nodal lines are phase dependent the nodal points remain fixed in space if ψ is multiplied by a constant phase factor $\exp(i\alpha)$. Thus we will focus on nodal points and their spatial distributions and try to characterize chaos in terms of such distributions. The question we wish to ask is simply if one can find a distinct difference between the distributions for nominally regular and irregular billiards [8].

In addition, which other signatures of quantum chaos may one find in the coherent transport in open billiards? Here we will choose to study numerically the general flow patterns derived from the probability currents associated with stationary scattering states. Nodal and saddle points and their spatial distributions play a decisive role in how the flow in the system is shaped. In this sense they are very physical. For example, it has been shown recently that quantum streamlines are effective concepts for understanding irregular conductance oscillations in two-dimensional rings [9].

II. NODAL LINES AND NODAL AND SADDLE POINTS

The scattering wave functions ψ for open billiards are found by solving the Schrödinger equation in a tight-binding approximation. The two-dimensional structures that we consider here consist of some specified cavity (e.g., a rectangle or Sinai billiard) with two attached semi-infinite leads. Electrons are confined by hard-wall boundaries and the interior potential is set equal to zero. Using the dimensionless variables

$$x \rightarrow x/d, \quad y \rightarrow y/d,$$

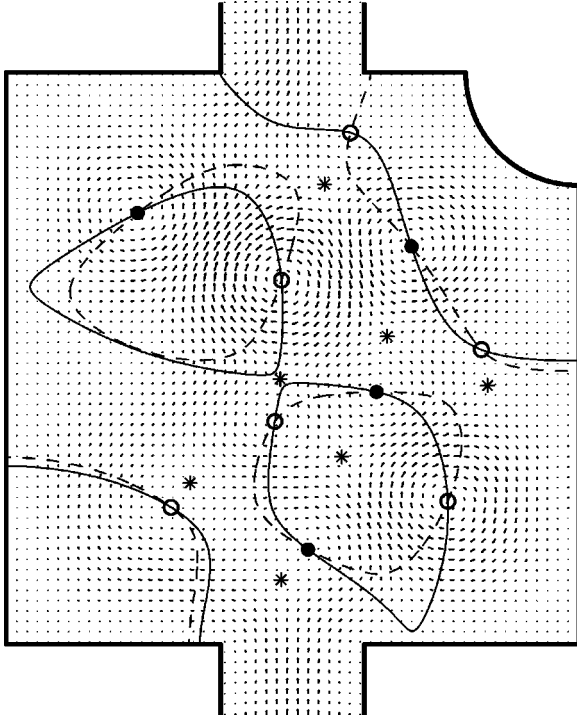


FIG. 1. Nodal lines, nodal and saddle points, and probability currents for electron transmission through a Sinai stadium with $\epsilon = 13$ (one transmission channel). The uNL ($\text{Re}[\psi] = u = 0$) are shown by solid lines and the vNL ($\text{Im}[\psi] = v = 0$) by dashed lines. The nodal points (NPs) are denoted by circles. Open circles refer to NPs with winding number $\sigma = 1$ while filled circles refer to $\sigma = -1$. The saddle points in the probability current flow are shown by stars. The particle is injected through the lower lead. The numerical dimensions of the Sinai billiard are 400×400 , $d = 100$, $R = 80$ where d is the width of the leads and R is the radius of the cutoff.

and energy

$$\epsilon = 2m^*d^2E/\hbar^2,$$

where d is the width of the leads, we map the Schrödinger equation for an electron of mass m^* onto a square lattice with $M \times N$ sites labeled (k, l) and with cell size a_0 . Below we will focus on the results for nodal properties and refer to Ref. [9] for details about the computational method.

A. The case of an open chaotic billiard

Figure 1 shows typical Chladni patterns for the nodal lines ($\text{Re}[\psi] = 0$ and $\text{Im}[\psi] = 0$), nodal points ($\psi = 0$), and saddle points (branching points in the current flow) for the scattering wave function in an open hard-walled Sinai billiard.

The energy of the incident electron in Fig. 1 is $\epsilon = 13$. At this energy there is only one open scattering channel in the leads. We let the incident state be a free particle state propagating along the straight lead times a transverse wave function. Moreover, the aspect ratio, i.e., ratio of the width of leads to the width of the billiard, is chosen so that the number of nodal points is relatively small. However, if we decrease the aspect ratio this number grows drastically as

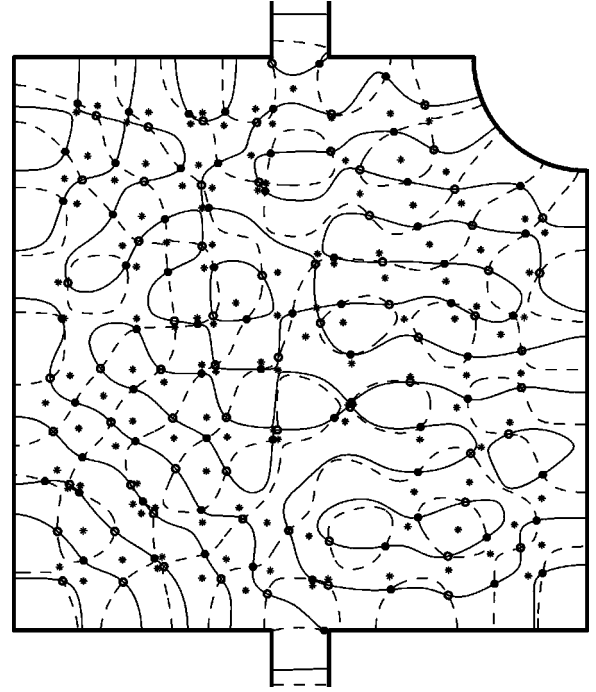


FIG. 2. Same as in Fig. 1 but for the Sinai billiard with numerical dimensions 500×500 , $R = 100$, $d = 50$, and $\epsilon = 20$. The numbers of saddle and nodal points ($\sigma = \pm 1$) are $N_{SP} = 127$ and $N_{\pm} = 68$, respectively.

shown in Fig. 2. The number of nodal points is approximately $\epsilon A / (4\pi d^2)$ where A is the area of the billiard.

Patterns of meandering, self-avoiding nodal lines that were already found theoretically by McDonald and Kaufman [3] for the isolated, irregular Bunimovich stadium are readily recovered here for both the imaginary and real parts of ψ . As mentioned already, the nodal lines for our complex scattering function are not uniquely defined because the constant phase α is arbitrary. Although the overall qualitative features look the same for different choices of α , i.e., there is the general picture of unidirectional and self-avoiding lines, they are not useful for a characterization of a complex chaotic wave function [4]. The nodal points, on the other hand, appear to be helpful in this respect because they stay invariant under the phase transformation α of the wave function.

B. Phase singularities

Explicit descriptions of the nodal points as phase singularities or topological charges associated with a complex wave function are given in many articles, for example, [10–18]. Let us write the wave function as

$$\psi(x, y) = \sqrt{\rho(x, y)} \exp i\theta(x, y), \quad (2)$$

where $\theta(x, y)$ and $\rho(x, y)$ denote the phase and norm. As Dirac demonstrated already in 1931 [10] nodal points give rise to current vortices. This means that when the following loop integral encloses a nodal point one has

$$\oint \mathbf{v} d\mathbf{r} = \oint \nabla \theta d\mathbf{r} = \pm 2\pi. \quad (3)$$

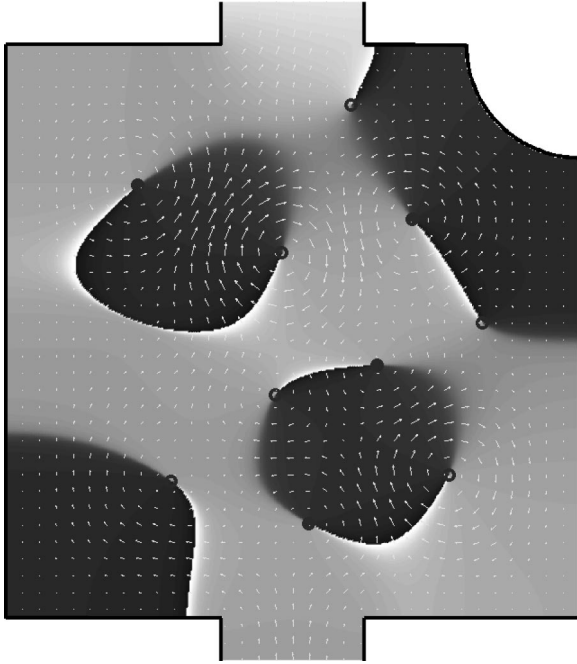


FIG. 3. The spatial pattern of the phase of the wave function for electron transmission through a Sinai billiard with the parameters given in Fig. 1. Sharp white/black lines correspond to 2π discontinuities in phase, which begin at a NP with σ and terminate at another NP with $-\sigma$ or proceed to the boundary of the system.

The quantum velocity \mathbf{v} is defined in terms of the probability current \mathbf{j} as

$$\mathbf{v} = \frac{\mathbf{j}}{\rho}, \quad \mathbf{j} = \text{Re}[\psi^* \mathbf{p} \psi] / m^*, \quad (4)$$

where $\mathbf{p} = -i\hbar \nabla$ is the momentum operator. The sign on the right hand side of formula (3) defines the winding number (WN). Relation (2) is illustrated in Fig. 3.

In the following discussion we will also use the alternative definition of the winding number [15,16]

$$\sigma = \text{sgn} \left(\frac{\partial u}{\partial x} \frac{\partial v}{\partial y} - \frac{\partial u}{\partial y} \frac{\partial v}{\partial x} \right), \quad (5)$$

where σ takes the values ± 1 for clockwise and counter-clockwise vortices as shown in Figs. 1 and 3. The relation between the phase of the wave function and the WN in Eq. (3) states that the phase undergoes a discontinuous change of $\pm 2\pi$ as one encircles a nodal point. Lines of phase discontinuity begin at one nodal point and terminate at another or proceed to the boundary of the system as illustrated in Fig. 3. Discontinuity lines of this kind have recently been obtained for microwave billiards for which the phase can be measured [19].

There is a close relation between nodal points with opposite WN as discussed in [16]. As shown in Figs. 1 and 2 a nodal line $u=0$ normally intersects a number of nodal lines $v=0$ and vice versa (for brevity “ u NL” and “ v NL,” respectively). Evidently neighboring nodal points on the same

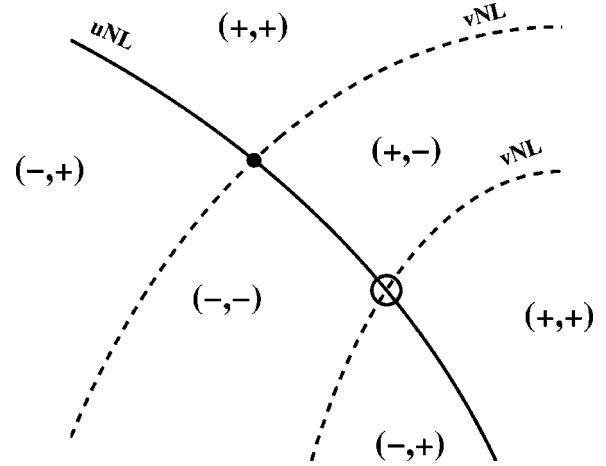


FIG. 4. An area with a u nodal line (u NL) intersected by two neighboring v nodal lines (v NL). Symbols $(\pm, \pm) = (\text{sgn}[u], \text{sgn}[v])$ indicate the sign of $u(x,y), v(x,y)$ in the different domains.

nodal line always have opposite WNs. To prove this we select a small domain in Fig. 2 in which two neighboring v NLs cross one u NL as in Fig. 4.

Introducing local Cartesian coordinates with the x axis along the tangent of the u NL we see that at the left nodal point $\partial u / \partial x = 0$ and therefore the first term in Eq. (5) vanishes. In the second term $\partial u / \partial y > 0$ and $\partial v / \partial x < 0$; hence $\sigma = 1$. For the nodal point to the right we get in the same way $\sigma = -1$. Obviously nodal points appear in pairs with opposite WNs. This means that they are created and annihilated in pairs when nodal lines evolve, for example, as energy and/or geometry change.

In contrast to the vortex lines the vortex centers remain fixed upon a change of constant phase factor α . As conjectured earlier [8] the nodal points may therefore serve as unique markers which should be useful for a quantitative characterization of scattering wave functions for open systems, i.e., they tell to what degree a system is chaotic.

C. Antivortices

Complementary to the vortices one finds in Figs. 1 and 3 that there is also a different kind of peculiarity in the current flow which is related to saddles [13,17], marked by stars. The saddle is a nodal point for the current. At such a point the “current nodal lines” $j_x = 0$ and $j_y = 0$ cross each other at nonzero u and v . Let us write the current density vector as $\mathbf{j}(x,y) = j(\cos \theta(x,y), \sin \theta(x,y))$ and then map the current phase $\theta(x,y)$ onto the angle ϕ which defines a circle $\mathbf{r} = r(\cos \phi, \sin \phi)$ of radius r around a point $\theta = \theta(\phi)$. If this circle encircles a vortex point then $\theta(2\pi) = 2\pi$ irrespective of the WN. On the other hand, if the circle embraces a saddle then $\theta(2\pi) = -2\pi$. For other cases $\theta(2\pi) = 0$. Therefore the saddles are often named antivortices.

D. The case of an open rectangular billiard

Figures 1 and 2 for a Sinai billiard set the stage for an open chaotic system with its typical disorder among the vor-

tices and antivortices. We now turn to the complementary case of a nominally regular system. The simplest choice to make is a rectangular billiard. It is instructive to first consider tunneling transport associated with a single isolated resonance peak. One finds essentially two different situations depending on whether the incident electron is in perfect resonance with the box or not.

The eigenfunctions and eigenvalues of a rectangle are well known. The dimensionless eigenvalues are $\epsilon_{mn} = \pi^2[m^2(d/L_x)^2 + n^2(d/L_y)^2]$ where L_x and L_y are the extensions of the rectangle and m and n are the quantum numbers $1, 2, 3, \dots$. For the closed rectangle the eigenfunctions ψ_{mn} are real and form a chessboard structure.

The coupling of the leads to the cavity can be governed by varying the hopping matrix element t connecting the rectangle and the leads. For a reduced coupling and in the vicinity of the conductance resonance $\epsilon \approx \epsilon_{mn}$ the scattering state in the interior region is mainly given by ψ_{mn} . Therefore, for the perfectly resonant case with $t=0.9$ the u NL and v NL will be only slightly distorted from a rectangular grid and stay close to each other as shown in Fig. 5(a). Consequently the nodal points will form an almost periodic lattice. This will also be the case for the antivortices.

If we now keep the above energy but open the box by increasing t in the coupling region we enhance the deformation of the nodal lines. We are still close, however, to resonant transmission. Consequently, the spatial structures of vortices and antivortices do not change appreciably as shown in Fig. 5(b) for $t=1$ although there is a rotation of phase α .

In order to change the positions of the vortices and antivortices the energy has to be changed as well. Figure 5(c) shows the case for $\epsilon = 15.1$ and $t=1$. The pattern is now less regular than for the resonant case $\epsilon = \epsilon_{mn}$.

On further deviation from the resonant energy the order will be reduced even more, i.e., the nodal point pattern will undergo profound changes from the crystalline to the amorphous. Does this mean that there might a gradual crossover from regular to chaotic behavior as leads are attached to an integrable billiard? If so, would the features of such a crossover be dependent on the particular choice of integrable billiard, rectangular, circular, or triangular? Would it also depend on the kind of attachment one makes?

III. DISTRIBUTION OF NODAL AND SADDLE POINTS

Following the discussion above we propose that an appropriate signature of quantum chaos in open cavities may be formulated in the following way. The distributions of distances between nearest nodal points are expected to be distinctly different for nominally regular and irregular billiards when the influence of the leads is small. For the regular lattice in Fig. 5, for example, one expects the distribution to be sharply peaked because the nodal points nearly form a crystal lattice. In contrast, Fig. 2 shows that there are no dominant distances between the nearest nodal points. The corresponding distribution should therefore be smeared.

To be quantitative we introduce four normalized distributions $P_{NP}(r)$, $P_{SP}(r)$, $P_{++}(r)$, and $P_{+-}(r)$ for the separations between nearest nodal points (NP), saddle points (SP),

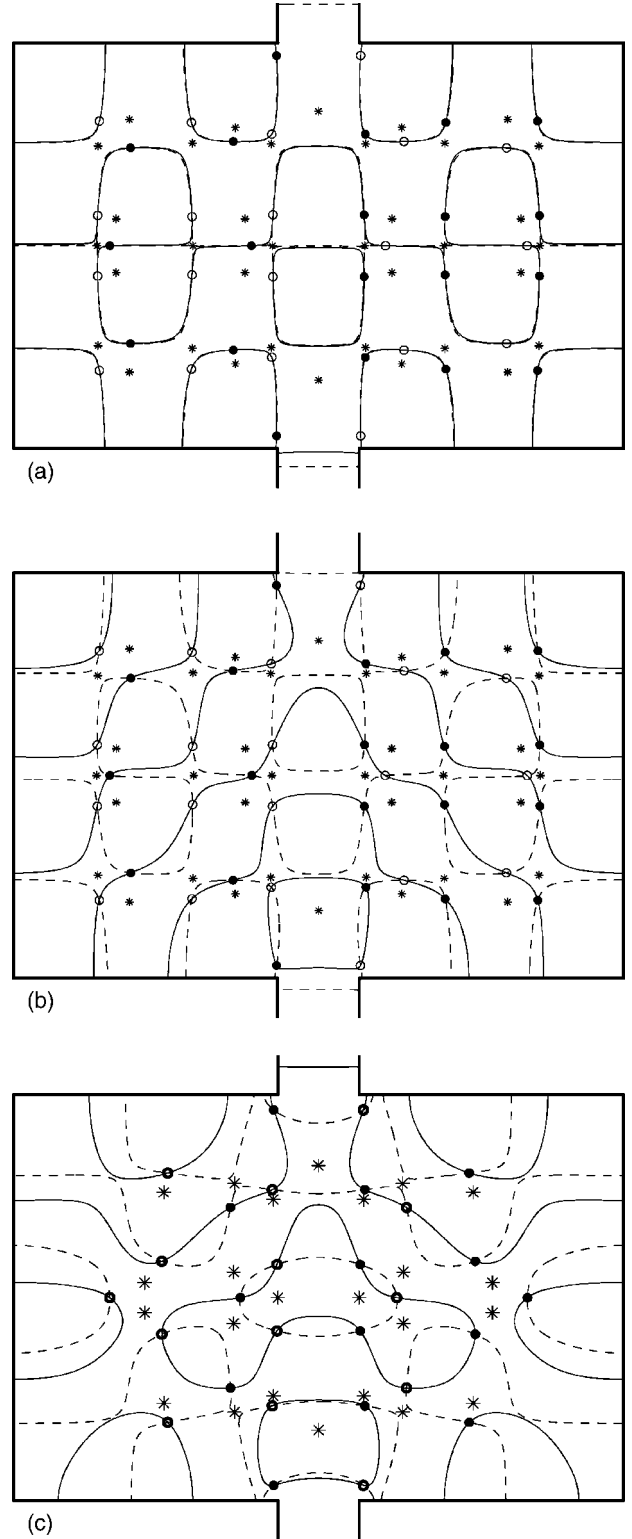


FIG. 5. Nodal lines and nodal and saddle points for transmission through a rectangular cavity with size 600×400 , $d=80$. (a) Tunneling regime with the hopping matrix elements $t=0.9$ connecting the leads to the cavity. The energy of the incident electrons, $\epsilon = 14.9126$, is tuned to maximum transmission ($T=1$) via the interior state with quantum numbers $m=7, n=4$. The u NL and v NL then almost coincide. (b) The same as for (a) but with $t=1$ and $T=0.98$. (c) The same as (b) but with $\epsilon=15.1$ and $T=0.8$.

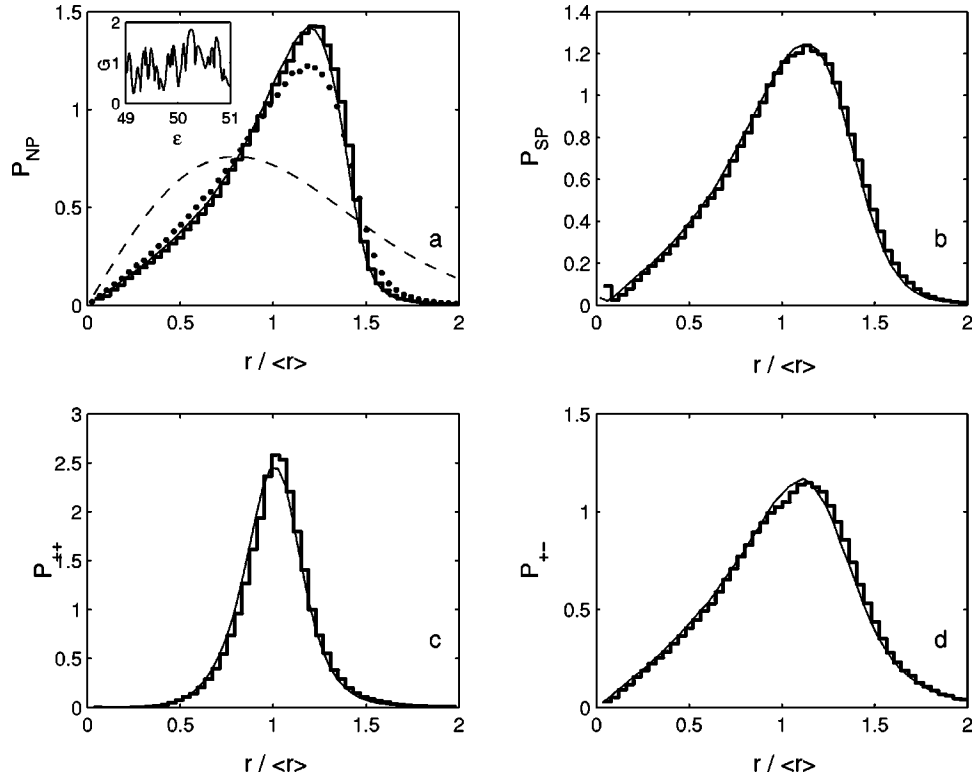


FIG. 6. Distributions $P_{NP}(r)$, $P_{SP}(r)$, $P_{++}(r)$, and $P_{+-}(r)$ for separations (in units of mean separation) between nearest nodal points (NP), saddle points (SP), and nodal points with the same ($++$) and opposite winding numbers ($+-$) in a chaotic Sinai billiard. The dimensions of the Sinai billiard and leads are 840×400 , $d=40$, and $R=40$. The distributions are found by averaging over 201 energies of the incident electrons, which results in the total number of points for the four cases $N_{NP}=635\,322$, $N_+=317\,765$, $N_-=317\,557$, and $N_{SP}=607\,045$. Two channels in the leads are open and the corresponding conductance fluctuations are shown in the inset in (a). The radial distribution (6) of nearest distances for completely random points is shown by the dashed curve in (a). The corresponding distributions for the Berry model function for a chaotic state (7) and random superposition (8) of 16 eigenfunctions for a rectangular box with the same size and energy are shown by dots and thin curves, respectively.

and nodal points with equal ($++$) and opposite ($+-$) winding numbers. For fixed energy $P_{++}(r) \neq P_{--}(r)$ and $P_{+-}(r) \neq P_{-+}(r)$ within the cavity because of its finite size. For an accumulation of statistics, however, $P_{++}(r) \rightarrow P_{--}(r)$ and $P_{+-}(r) \rightarrow P_{-+}(r)$. We chose the following averaging over distributions. Since the spatial distribution of the nodal points may be sensitive to whether the energy of the incident electron is resonant or not we accumulate statistical samples by sweeping the energy over an energy window that contains at least a few resonant transmission peaks. As our computer calculations show, differences between $P_{++}(r)$ and $P_{--}(r)$ then disappear. We will also consider the case that the positions and shapes of the leads are altered.

A. Case of chaotic cavities

The distributions $P_{NP}(r)$, $P_{SP}(r)$, $P_{++}(r)$, and $P_{+-}(r)$ of the open Sinai billiard are shown in Fig. 6. Two transverse modes are open in the leads. The distributions are obtained as the average over 201 different energies within the energy window between $\epsilon=49$ and $\epsilon=50$. This energy window is wide enough to include a number of conductance oscillations as shown in the inset of Fig. 6(a). The total number of nodal points with specific winding number and the total number of saddle points are given in the figure caption.

We have also considered other cases of averaging, such as over different energy windows and positions of leads, and the influence of wider leads. In all these cases the distributions of nearest neighbors were practically the same as in Fig. 6. We therefore argue that there are generic distributions for nearest neighbor separations which may be taken as signatures of wave chaos [8].

Figure 6 shows the general result that nodal points with opposite WN have a tendency to attract each other, while points with equal WNs repel. Hence quantum chaos is not the same as complete randomness. This is also evident from the distribution for nearest neighbors among random points [20]

$$P(r) = \frac{\pi}{2} r \exp(-\pi r^2/4), \quad (6)$$

where r is the separation between points in units of the mean separation $\langle r \rangle$. The distribution is shown for comparison in Fig. 6(a). The distinct difference between the curves thus demonstrates that there is an underlying correlation between the nodal points in the irregular cavity. Figure 6(d), finally, shows the distribution of nearest distances between the saddle points. This distribution is apparently quite close to

$P_{+-}(r)$. As will be seen below, $P_{NP}(r)$ is the distribution that is most sensitive to geometry. To test the idea of generic distributions further we have investigated variations of the Sinai billiard with the same results. We have also considered the irregular Bunimovich billiard [21]. Except for slight numerical deviations, the Bunimovich billiard gives rise to the same distributions as the Sinai billiard.

B. The Berry wave function and complex combination states

There is a simple way to understand the nature the generic distribution above. Intuitively a wave chaotic state may be viewed as a random superposition of monochromatic plane wave states. For any point not too close to the boundary of a billiard and for Fermi wavelengths much smaller than the dimensions of the enclosure, we thus assume that we may approximate the true state with the Berry conjecture [22]

$$\psi(x,y) = \sum_j a_j \exp[i(\mathbf{k}_j \cdot \mathbf{r} + \phi_j)] \quad (7)$$

where a_j and ϕ_j are independent random real variables and \mathbf{k}_j are randomly oriented wave vectors of equal length.

Correlation functions [18,23] for nodal points and the different distributions $P_{NP}(r)$, $P_{++}(r)$, and $P_{+-}(r)$ for the Berry function have been considered previously [23,24]. The dotted curve in Fig. 6 shows the results for $P_{NP}(r)$, which are typical also for the remaining distributions. The qualitative picture is indeed quite satisfactory. In spite of numerical deficiencies, in particular around the peak values, the Berry state apparently provides a key for understanding the distributions in a Sinai billiard.

As mentioned the Berry function should be a good representation of the true scattering state for points not too close to the boundaries [25]. On the other hand, whenever finite size and the boundaries play a role the probability for large separations between nearest points is reduced. Because the distributions $P_{NP}(r)$ in Fig. 6(a) are normalized, a reduction in the high tail is compensated by an increase in the dominant peak region, as shown by the figure. As an easy remedy for boundary effects we therefore modify the Berry function as [21]

$$\psi(x,y) \approx \sum_{mn} a_{mn} \psi_{mn}(x,y), \quad (8)$$

where $\psi_{mn}(x,y)$ are the eigenstates of a closed rectangular cavity and the mixing coefficients $\text{Re}(a_{mn})$ and $\text{Im}(a_{mn})$ are independent random Gaussian variables. These kinds of ‘‘combination state’’ are also known from other parts of wave physics. The summation in Eq. (8) includes states within a narrow energy window, i.e., a number of reshuffled and ‘‘lifetime broadened,’’ nearly monochromatic states are allowed to mix when there are many open channels and/or the energy is high. In principle we should sum over the eigenfunctions of the Sinai billiard but these are computationally cumbersome. In doing so we would also lose the

simplicity of Eq. (8). Since the rectangle coincides with the Sinai billiard except for the rounded corner this difference may be ignored.

The Berry function in Eq. (7) represents a random Gaussian complex field. The function (8) may also be considered as such a field provided the number of superposed states is large enough. As indicated, the expansion (8) is limited to states within a small energy window around ϵ . In practice, superpositions of 16 or 24 states approximate a random field rather well. As a consequence we do not find any visible differences in the distributions displayed in Fig. 6 with these two choices. In a statistical sense our modified combination states thus represent the true interior chaotic scattering state quite well. As a consequence the corresponding distributions of nodal points and antivortices are also well described within this framework.

C. Case of rectangular cavities

Let us now turn to the case of nominally regular cavities and how leads affect the different statistical distributions. We chose an open rectangle as an example of such a billiard because it is the limiting case of the Sinai billiard as the radius $R \rightarrow 0$ for the cut corner. Figure 7 shows the distributions at two-channel transmission with the same energy averaging procedure as for the Sinai billiard. The distribution $P_{NP}(r)$ clearly displays a central peak corresponding to partial order among the nodal points and is therefore distinctly different from the Sinai case. The height of the distribution P_{++} indicates that the partial order relates to nodal points. This is also the case at much higher energies. On the other hand, the distribution for saddle points, P_{SP} in Fig. 7, shows little difference from the chaotic case. We take this to mean that P_{SP} is a less useful discriminator and will not consider it further.

One may suspect that a reason for the partial regularity among the nodal points is due to the symmetric attachment of leads. We have therefore considered P_{NP} also for asymmetric positions of leads. Moreover we performed an average over positions of the input lead at fixed energy. In all cases the signs of partial order remain. Therefore an open rectangular billiard with two straight sharp-cornered leads displays robustness and considerable regularity among the nodal points. Consequently the various attachments of leads do not turn regularity into chaos in this case.

D. Analysis of the numerical scattering states

In order to understand the above features of the distributions let us find the coefficients a_{mn} in the function (8) by projecting the numerical scattering functions on the eigenfunctions ψ_{mn} . A typical case is shown in Fig. 8. As anticipated the expansion is heavily dominated by eigenstates ψ_{mn} with effectively the same energies ϵ_{mn} as the incoming electron [26]. Hence the coefficients $|a_{mn}|^2$ in the (m,n) plots in Fig. 8 fall more or less on an elliptic curve. The specific composition of eigenstates and nodal points may, however, change swiftly with energy.

Figure 8 pinpoints a key difference between the regular rectangular and the chaotic Sinai billiards. Evidently there

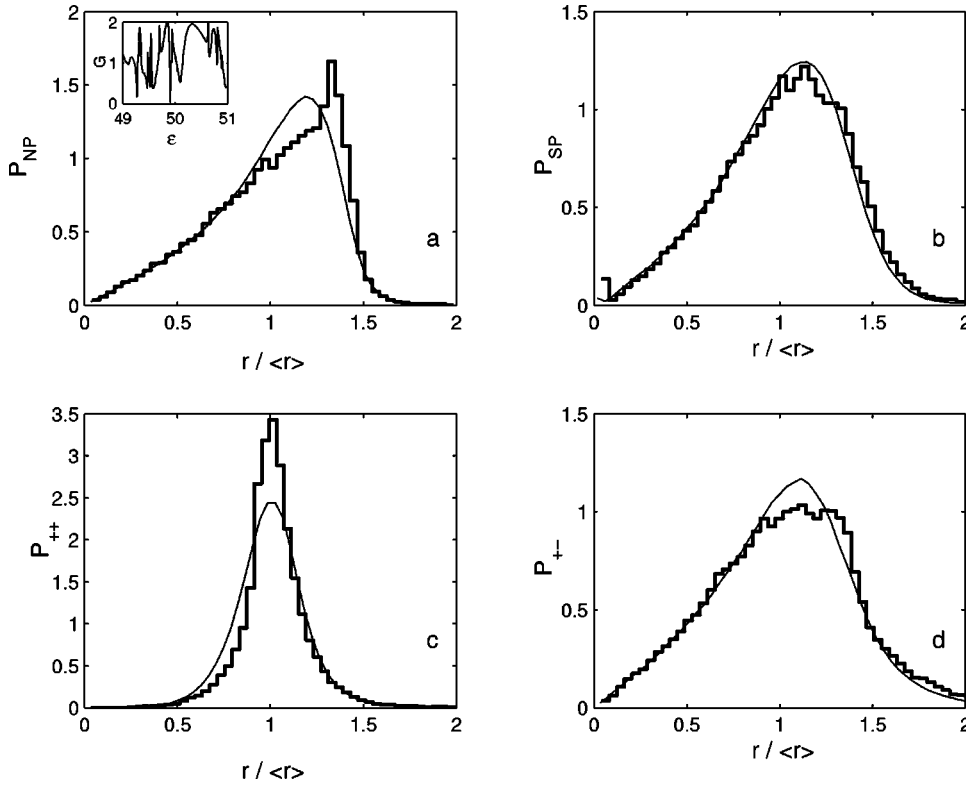


FIG. 7. Energy averaged distributions $P_{NP}(r)$, $P_{SP}(r)$, $P_{++}(r)$, and $P_{+-}(r)$ for an open rectangle at two-channel transmission. The entrances of leads form sharp corners and are positioned as in Fig. 5. The total numbers of points included in the statistics are $N_{NP}=619\,158$, $N_+=309\,563$, $N_-=309\,595$, and $N_{SP}=583\,288$. The distributions for the random combination state (8) with 16 randomly superposed eigenfunctions for the rectangle are shown by the thin curves. The dimensions of the system are 840×400 and $d=40$.

are only a few dominant eigenstates that constitute the scattering wave function, too few to make a chaotic state as in Fig. 6. The question is, therefore, how to increase the number of contributions if one wants the system to cross over to chaos. One may think that a widening of the leads and/or an increase of the energy would engage more eigenstates. Our experience shows, however, that the number of dominant states stays small in either case. Consequently the rectangular billiard with sharp-cornered leads does not cross over to irregular behavior.

E. Role of soft leads

In the above analysis of a rectangular billiard we have found that only a few dominant eigenstates contribute to the transmission. Figure 8 shows, however, that there are more states available along the elliptic curve. Sharp-cornered leads are evidently too selective. The question is how to get all the states engaged on equal footing and thereby reach a richer combination state.

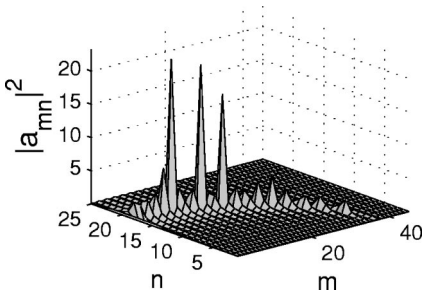


FIG. 8. Relative weights $|a_{mn}|^2$ of the eigenstates ψ_{mn} participating in the electron transmission through a rectangular billiard with size 840×400 , $d=40$, and energy $\epsilon=40$.

One way to achieve a better mixing of states is to alter the shape of the leads. If we replace the sharp corners by rounded or flared ones the injection into the billiard will be more collimated [27]. We should therefore expect a broader representation of eigenstates with large weight $|a_{mn}^2|$. The choice of rounded corners, for example, is a natural one for ballistic semiconductor devices in which depletion effects normally gives rise to smeared features.

Figure 9 shows P_{NP} for the rectangular billiard with the same dimensions and averaging procedure as in Fig. 7. Obviously the features related to partial ordering of nodal points have now disappeared and P_{NP} is close to the generic form found for the chaotic Sinai billiard. We may therefore say that there is a crossover to irregularity as we insert rounded or flared contacts. Multiple probes would accelerate such a crossover.

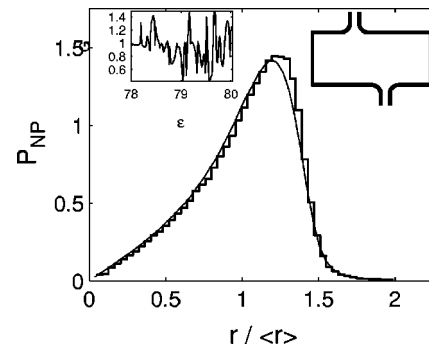


FIG. 9. Histogram for rounded asymmetric leads as shown in the insets. P_{NP} for the Sinai billiard is also shown. The radius of the rounded sections is $R \sim d$.

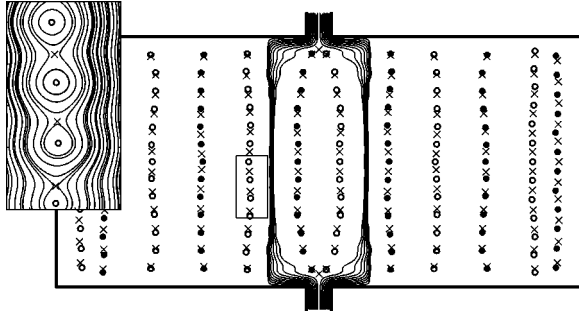


FIG. 10. Streamlines for the net flow and positions of nodal points with different winding numbers (open and filled circles) and saddle points (\times) in a rectangle of size 420×200 and $d=20$ at resonant transmission: $\epsilon=19.2727$, $t=0.75$. The magnification shows streamlines for the indicated “interior” region, which does not contribute to the net flow.

IV. QUANTUM STREAMLINES

The vortices and antivortices are intimately connected with current flow. Vortices play the role of impurities which the net current through the system must circumvent. Antivortices act as beam splitters. To get further insight it is useful to analyze velocity fields and streamlines. We therefore consider the velocity \mathbf{v} as defined in Eq. (4)

$$\mathbf{v} = \dot{\mathbf{x}} = \hbar \nabla \theta / m^*, \quad (9)$$

which integrated over time gives the streamlines. The quantum streamlines are sometimes referred to as Bohm trajectories [28]. In this alternative interpretation of quantum mechanics an electron is viewed as a “real” particle in the classical sense, following a continuous and causally defined trajectory (streamline) with a well defined position \mathbf{x} and velocity \mathbf{v} . The electron is thought to move under the action of a force which is not obtained entirely from the classical potential V , but also contains a “quantum mechanical” potential

$$V_{QM} = -\frac{\hbar^2}{2m^*} \frac{\nabla^2 \rho^{1/2}}{\rho^{1/2}}. \quad (10)$$

This quantum potential is negatively large where the wave function is small, and becomes infinite at the nodal points. Therefore, the close surrounding of a nodal point is forbidden for the quantum streamlines contributing to the net transport from source to drain. One may say that the nodal points effectively act as impenetrable impurities with the same extensions as the vortices. Moreover, the nodal points are topological singularities of the wave function; therefore “open” streamlines associated with the net current cannot encircle a nodal point.

As seen from Fig. 2 the nodal points for the Sinai billiard are disordered while for the rectangular case in Fig. 5 they may form a “nodal crystal.” We should therefore expect different behavior for the quantum streamlines for these two cases. Figure 10 shows the flow lines (Bohm trajectories) in the case of the rectangular cavity. The general features of the flow lines connecting input and output leads are remarkable.

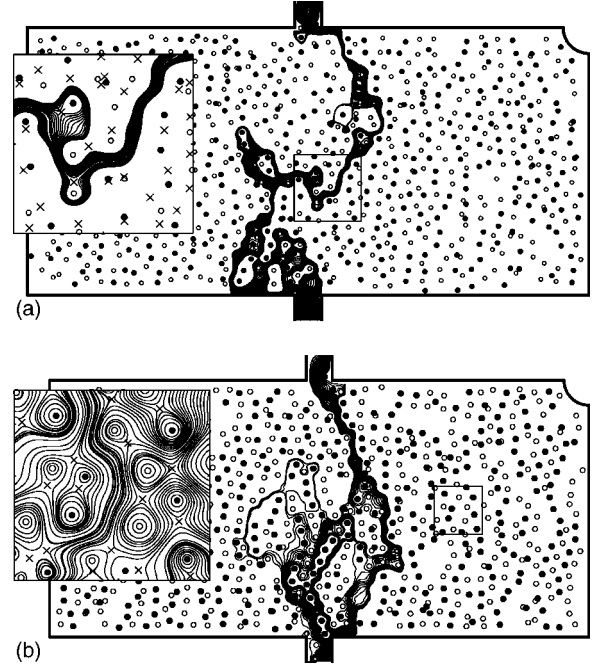


FIG. 11. Streamlines for the net flow and positions of nodal points with different winding numbers (open and filled circles) for a Sinai billiard at energy 49.9 (upper case) and 50.0 (lower case). Two channels are open. Sizes of billiard and leads are the same as in Fig. 6. The inset in the upper case shows a magnification of the net flow in the region indicated by a square. Crosses denote saddle points. The inset in the lower panel shows the whirling closed streamlines for the indicated “interior” region, which does not contribute to the net flow.

It is clearly seen how the flow of particles (trajectories) effectively “channel” through the nodal crystal. The saddle points at the contacts act as branching points. This picture is evidently very different from semi-classical physics and periodic orbit theory [29]. The contributions to the net current are displayed in Fig. 10 and the following figures. In addition there are also closed vortical motions around the nodal points as described above and illustrated by the insets in Figs. 10

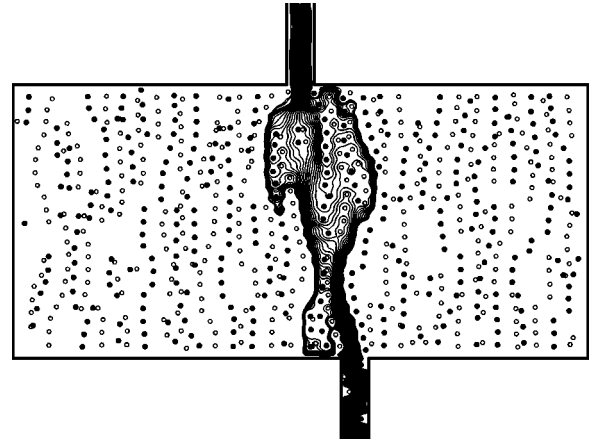


FIG. 12. Streamlines for the net flow through a rectangle with sharp corners at energy 50.1. The dimensions are the same as in Fig. 7. The offset of the input lead is $2d$.

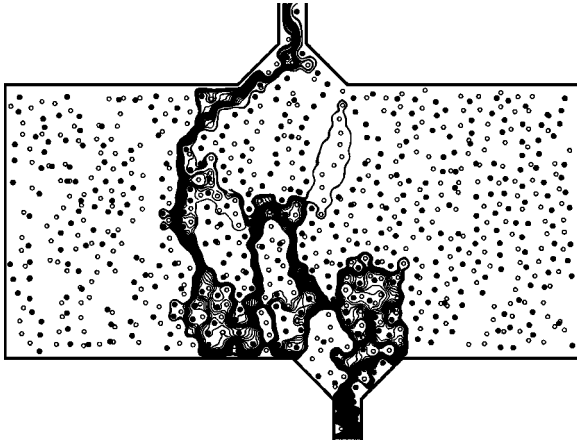


FIG. 13. Same as in Fig. 12 but with flared leads, effectively of the same size as the rounded leads in Fig. 9.

and 11. The net current through the billiard is actually rather small compared with the flow absorbed in the vortical motions. To a good approximation one may then work out current statistics using the random functions in Sec. III B. If we choose the Berry function this can be done analytically [30].

As seen from Fig. 10 saddle points are also important because they are related to spatial instabilities of the streamlines leading to the branching of the injected beam. As for the vortices we may regard the antivortices as scatterers. In Fig. 10 the branching takes place near the entrance. The “particles” then channel through the nodal crystal.

If we now go to the complementary case, the Sinai billiard in Fig. 11, the streamlines look extremely complex. Because the distributions of nodal points are irregular the streamlines also form an irregular pattern when finding their way through the potential landscape. Figure 11 and the following figures bring to mind the classical example of meandering rivers in a flat delta landscape. As is well known, slight changes in the topography, for example, by moving only a few stones to new positions, may induce different flow patterns in sometimes dramatic ways. In the same way slight variations of the energy, for example, affect the quantum streamlines in an endless way. Figure 11 shows two cases which differ in energy by only 0.2%.

Let us now return to the rectangular billiard in Fig. 10 but let the energy be much higher and assume asymmetric positions of the leads. One notices in Fig. 12 that the nodal points are still partially ordered in accordance with the discussions above. Because of this we find traces of channeling in open “corridors.” Figure 13 shows the importance of the shape of the contact regions. As is to be expected, flared contacts break up the ordering among nodal points in the previous figure and spread the flowlines.

In all the complex figures above there are regions between strands with opposite winding numbers. A net current flow occurs when there are regions that happen to connect the two leads. This feature recalls percolation and we suggest that this might be an alternative useful way to analyze irregular transport through an open billiard.

V. SUMMARY AND CONCLUDING REMARKS

We have considered quantum ballistic transport in some typical two-dimensional open billiards which are nominally

integrable or nonintegrable. We have emphasized the role of vortices and antivortices in the scattering wave function and illustrated how the array of such points is intimately related to the net current flow through a ballistic billiard. Depending on the geometry, energy of an injected particle, positions and shapes of leads, etc., a rich variety of flow patterns or quantum trajectories is found, ranging from channeling to volatile situations in which the flow lines may rearrange swiftly after small changes. In this sense there is an analogy with classical chaos as to the extreme sensitivity of trajectories. Figure 11 shows how the quantum trajectories may change drastically on only a tiny change $\Delta\lambda$ of the wavelength λ . In the limit of very small λ , as in the semiclassical limit, effects of this kind can become very dramatic. The spacing between nodal points is roughly equal to λ . Thus as $\lambda \rightarrow 0$ even infinitesimal alterations in, for example, lead positions will induce new flow patterns that are not foreseeable. We have also suggested that percolation theory might be useful for analyzing these features.

We have also argued that there are generic distribution functions for the nearest separations between vortices in irregular open systems. The distributions may thus be taken as a signature of quantum chaos and may be used for diagnostic purposes. We have used these distributions to find out about the effects of leads attached to a regular billiard, in our case a rectangle. In general, leads induce disorder among the nodal points although preferred directions may still remain as in Fig. 12. If contacts excite more eigenmodes, as in the case of rounded or flared contacts, there is a crossover to distributions that are generic for chaotic billiards. The matter is not the shape of the billiard but how many eigenmodes of the billiard couple to the leads.

The phenomena we have discussed here derive from general properties of waves and are therefore not unique to quantum mechanics. There is, for example, a close similarity with planar electromagnetic wave guides and cavities [1]. The basic equations take the same form and, in particular, the Poynting vector is the analog of the quantum mechanical current. It should therefore be possible to observe experimentally nodal points and streamlines in microwave billiards [19,31]. In principle, these phenomena could also be observed in wave transmission in other analogous macroscopic systems [32]. In particular, the conjecture of generic forms for the nearest neighbor separations might be tested experimentally. The close relation between relative positions of nodal points, vorticity, channeling, and meandering chaotic streamlines might also be observed. It is promising also that experimental techniques to image coherent electron flows through semiconductor nanostructures are becoming available using scanned probe microscopes [33,34].

ACKNOWLEDGMENTS

This work was partially supported by the Royal Swedish Academy of Sciences (A.F.S) and by the Russian Foundation for Basic Research Grant No. 01-02-16077 (A.F.S. and A.A.S). The computations were in part performed at the National Supercomputer Centre at Linköping University.

- [1] See, e.g., H.-J. Stöckmann, *Quantum Chaos: An Introduction* (Cambridge University Press, Cambridge, U.K., 1999), and references cited therein.
- [2] J.H. Davies, *The Physics of Low-Dimensional Structures* (Cambridge University Press, Cambridge, U.K., 1998).
- [3] S.W. McDonald and A.N. Kaufman, Phys. Rev. Lett. **42**, 1189 (1979); Phys. Rev. A **37**, 3067 (1988).
- [4] Noncrossing nodal lines may also be found in, for example, a regular square two-dimensional billiard by a suitable linear combination of degenerate solutions. Therefore noncrossing would not be a consequence of chaos. [See, e.g., M. Berry, in *Chaotic Behavior of Deterministic Systems*, Les Houches Summer School in Theoretical Physics, 1981, edited by G. Iooss, R.H.G. Helleman, and R. Stora (North-Holland, Amsterdam, 1983)]. However, a basic property of nonintegrable systems, like the Sinai billiard, is that states are nondegenerate and the associated nodal pattern is unidirectional and disordered as well as self-avoiding. In contrast to the square, for example, there is no simple linear transformation among degenerate states that would restore a regular pattern of crossing nodal lines.
- [5] E. Bogomolny and C. Schmit, Phys. Rev. Lett. **88**, 114102 (2002).
- [6] S. Sridhar and E. Heller, Phys. Rev. A **46**, R1728 (1992).
- [7] C. Ellegaard, K. Schaadt, and P. Bertelsen, Phys. Scr., T **T90**, 223 (2001).
- [8] K.-F. Berggren, K.N. Pichugin, A.F. Sadreev, and A.A. Starikov, JETP Lett. **70**, 403 (1999).
- [9] K.N. Pichugin and A.F. Sadreev, Phys. Rev. B **56**, 9662 (1997).
- [10] P.A.M. Dirac, Proc. R. Soc. London, Ser. A **133**, 60 (1931).
- [11] J.F. Nye and M.V. Berry, Proc. R. Soc. London, Ser. A **336**, 165 (1974).
- [12] J.O. Hirschfelder, A.C. Christoph, and W.E. Palke, J. Chem. Phys. **61**, 5435 (1974).
- [13] J.O. Hirschfelder, C.J. Goebel, and L.W. Bruch, J. Chem. Phys. **61**, 5456 (1974).
- [14] M. V. Berry, in *Physics of Defects*, edited by R. Balian *et al.* (North-Holland, Amsterdam, 1981).
- [15] B.I. Halperin, in *Physics of Defects* (Ref. [14]).
- [16] N. Shvartsman and I. Freund, Phys. Rev. Lett. **72**, 1008 (1994).
- [17] H. Wu and D.W.L. Sprung, Phys. Lett. A **183**, 413 (1993).
- [18] M.V. Berry and M.R. Dennis, Proc. R. Soc. London, Ser. A **456**, 2059 (2000).
- [19] M. Barth, Ph.D. thesis, Fachbereich Physik der Philipps-Universität Marburg, Marburg/Lahn, 2001.
- [20] J.R. Eggert, Phys. Rev. B **29**, 6664 (1984).
- [21] For a preliminary report, see K.-F. Berggren, A.F. Sadreev, and A.A. Starikov, Nanotechnology **12**, 562 (2001).
- [22] M.V. Berry, Philos. Trans. R. Soc. London, Ser. A **287**, 237 (1977).
- [23] A.I. Saichev, K.-F. Berggren, and A.F. Sadreev, Phys. Rev. E **64**, 036222 (2001); **65**, 019903(E) (2002).
- [24] M.R. Dennis, Proc. SPIE **4403**, 13 (2001).
- [25] Recently Berry has considered perimeter corrections for mean density of nodal points, fluctuations, and curvatures: M.V. Berry, J. Phys. A **35**, 3025 (2002).
- [26] I.V. Zozoulenko and K.-F. Berggren, Phys. Rev. B **56**, 6931 (1997).
- [27] C.W. Beenakker and H. van Houten, in *Solid State Physics Quantum Transport in Semiconductor Nanostructures*, edited by H. Ehrenreich and D. Turnbull (Academic Press, New York, 1991), Vol. 44.
- [28] J. Baggott, *The Meaning of Quantum Theory* (Oxford University Press, Oxford, 1993).
- [29] M. Brack and R.K. Bhaduri, *Semiclassical Physics* (Addison-Wesley, Reading, MA, 1997).
- [30] A.I. Saichev, H. Ishio, A.F. Sadreev, and K.-F. Berggren, J. Phys. A **35**, L87 (2002).
- [31] M. Barth and H.-J. Stöckmann, Phys. Rev. E **65**, 066208 (2002).
- [32] See, for example, F.J. Fahy, *Sound Intensity*, 2nd ed. (E & FN Spon, London, 1995).
- [33] M.A. Topinka, B.J. LeRoy, S.E.J. Shaw, E.J. Heller, R.M. Westerwelt, K.D. Maranowski, and A.C. Gossard, Science **289**, 2323 (2000).
- [34] M.A. Topinka, B.J. LeRoy, R.M. Westerwelt, S.E.J. Shaw, R. Fleischman, E.J. Heller, K.D. Maranowski, and A.C. Gossard, Nature (London) **410**, 183 (2001).